# We are IntechOpen, the world's leading publisher of Open Access books Built by scientists, for scientists

**4,800**
Open access books available

**122,000**
International authors and editors

**135M**
Downloads

Our authors are among the

**154**
Countries delivered to

**TOP 1%**
most cited scientists

**12.2%**
Contributors from top 500 universities

CLARIVATE ANALYTICS BOOK CITATION INDEX INDEXED

WEB OF SCIENCE™

Selection of our books indexed in the Book Citation Index in Web of Science™ Core Collection (BKCI)

## Interested in publishing with us?
## Contact book.department@intechopen.com

Numbers displayed above are based on latest data collected.
For more information visit www.intechopen.com

# 7

# Quantitative Feedback Theory and Sliding Mode Control

Gemunu Happawana
*Department of Mechanical Engineering,*
*California State University, Fresno, California*
*USA*

## 1. Introduction

A robust control method that combines Sliding Mode Control (SMC) and Quantitative Feedback Theory (QFT) is introduced in this chapter. The utility of SMC schemes in robust tracking of nonlinear mechanical systems, although established through a body of published results in the area of robotics, has important issues related to implementation and chattering behavior that remain unresolved. Implementation of QFT during the sliding phase of a SMC controller not only eliminates chatter but also achieves vibration isolation. In addition, QFT does not diminish the robustness characteristics of the SMC because it is known to tolerate large parametric and phase information uncertainties. As an example, a driver's seat of a heavy truck will be used to show the basic theoretical approach in implementing the combined SMC and QFT controllers through modeling and numerical simulation. The SMC is used to track the trajectory of the desired motion of the driver's seat. When the system enters into sliding regime, chattering occurs due to switching delays as well as systems vibrations. The chattering is eliminated with the introduction of QFT inside the boundary layer to ensure smooth tracking. Furthermore, this chapter will illustrate that using SMC alone requires higher actuator forces for tracking than using both control schemes together. Also, it will be illustrated that the presence of uncertainties and unmodeled high frequency dynamics can largely be ignored with the use of QFT.

## 2. Quantitative Feedback Theory Preliminaries

QFT is different from other robust control methodologies, such as LQR/LTR, mu-synthesis, or $H_2$/ $H^\infty$ control, in that large parametric uncertainty and phase uncertainty information is directly considered in the design process. This results in smaller bandwidths and lower cost of feedback.

### 2.1 System design

Engineering design theory claims that every engineering design process should satisfy the following conditions:

1. Maintenance of the independence of the design functional requirements.
2. Minimization of the design information content.

For control system design problems, Condition 1 translates into approximate decoupling in multivariable systems, while Condition 2 translates into minimization of the controller high frequency generalized gain-bandwidth product (Nwokah et al., 1997).
The information content of the design process is embedded in G, the forward loop controller to be designed, and often has to do with complexity, dimensionality, and cost. Using the system design approach, one can pose the following general design optimization problem. Let **G** be the set of all G for which a design problem has a solution. The optimization problem then is:

$$\underset{G \in \mathbf{G}}{Minimize} \ \{Information\ \ content of G\}$$

subject to:
i. satisfaction of the functional requirements
ii. independence of the functional requirements
iii. quality adequacy of the designed function.
In the context of single input, single output (SISO) linear control systems, G is given by:

$$I_c = \int_0^{\omega_G} \log|G(i\omega)|\, d\omega \ , \tag{1}$$

where $\omega_G$ is the gain crossover frequency or effective bandwidth. If **P** is a plant family given by

$$\mathbf{P} = P(\lambda,s)\left[1+\Delta\right] \ , \ \lambda \in \Lambda \ , \ \Delta \in H^{\infty} \ , \ |\Delta| < W_2(\omega) \ , \tag{2}$$

then the major functional requirement can be reduced to:

$$\eta\left(\omega,\lambda,G(i\omega)\right) = W_1(\omega)|S(\lambda,i\omega)| + W_2(\omega)|T(\lambda,i\omega)| \le 1 \ ,$$

$\forall \omega \ge 0$ , $\forall \lambda \in \Lambda$ , where $W_1(\omega)$ and $W_2(\omega)$ are appropriate weighting functions, and S and T are respectively the sensitivity and complementary sensitivity functions. Write

$$\bar{\eta}\left(\omega,G(i\omega)\right) = \max_{\lambda \in \Lambda} \eta\left(\lambda,\omega,G(i\omega)\right) .$$

Then the system design approach applied to a SISO feedback problem reduces to the following problem:

$$I_c^* = \min_{G \in \mathbf{G}} \int_0^{\omega_G} \log|G(i\omega)|\, d\omega \ , \tag{3}$$

subject to:
i. $\bar{\eta}\left(\omega,G(i\omega)\right) \le 1$ , $\forall \omega \ge 0$ ,
ii. quality adequacy of $T = \dfrac{PG}{1+PG}$.

Theorem: Suppose $G^* \in \mathbf{G}$ . Then:

$I_c^* = \min_{G \in \mathbf{G}} \int_0^{\omega_G} \log|G|\, d\omega = \int_0^{\omega^*_G} \log|G^*|\, d\omega$ if and only if $\bar{\eta}\left(\omega, G^*(i\omega)\right) = 1, \forall \omega \geq 0$.

The above theorem says that the constraint satisfaction with equality is equivalent to optimality. Since the constraint must be satisfied with inequality $\forall \omega \geq 0$; it follows that a rational $G^*$ must have infinite order. Thus the optimal $G^*$ is unrealizable and because of order, would lead to spectral singularities for large parameter variations; and hence would be quality-inadequate.

Corollary: Every quality-adequate design is suboptimal.

Both $W_1, W_2$ satisfy the compatibility condition $\min\{W_1, W_2\} < 1$, $\forall \omega \in [0, \infty]$. Now define

$$\bar{\eta}(\omega, G(i\omega)) = \max_{\lambda \in \Lambda} \eta(\omega, \lambda, G(i\omega)) \Leftrightarrow \bar{\eta}(\omega, G(i\omega)) \leq 1, \forall \omega \in [0, \infty]. \tag{4}$$

Here $W_1(\omega) \geq 0 \in L_1$ or in some cases can be unbounded as $\omega \to 0$, while $W_2(\omega) \in L_2$, and satisfies the conditions:

$$\text{i.} \quad \lim_{\omega \to \infty} W_2(\omega) = \infty, \; W_2 \geq 0,$$

$$\text{ii.} \quad \int_{-\infty}^{+\infty} \frac{|\log W_2(\omega)|}{1 + \omega^2}\, d\omega < \infty. \tag{5}$$

Our design problem now reduces to:

$$\min_{G \in \mathbf{G}} \int_0^{\omega_G} \log|G(i\omega)|\, d\omega,$$

subject to:

$$\bar{\eta}(\omega, G(i\omega)) \leq 1, \forall \omega \in [0, \infty].$$

The above problem does not have an analytic solution. For a numerical solution we define the nominal loop transmission function

$$L_0(i\omega) = P_0 G(i\omega),$$

where $P_0 \in \mathbf{P}$ is a nominal plant. Consider the sub-level set $\Gamma : \mathbf{M} \to \mathbf{C}$ given by

$$\Gamma(\omega, G(i\omega)) = \{P_0 G : \bar{\eta}(\omega, G(i\omega)) \leq 1\} \subset \mathbf{C}, \tag{6}$$

and the map

$$f(\omega, W_1, W_2, \phi, q) : M \to \Gamma(w, G(i\omega)),$$

which carries $\mathbf{M}$ into $\Gamma(\omega, G(i\omega))$.

Also consider the level curve of $(\Gamma(\omega, G(i\omega)))$ $\partial\Gamma : \mathbf{M} \rightarrow \mathrm{C} \setminus \{\infty\}$ given by,

$$\partial\Gamma(\omega, G(i\omega)) = \{P_0 G : \bar{\eta}(\omega, G(i\omega)) = 1\} \subset \mathbf{C} \setminus \{\infty\} .$$

The map

$$f : \mathbf{M} \rightarrow \partial\Gamma(\omega, G(i\omega)) \subset \mathbf{C} ,$$

generates bounds on **C** for which f is satisfied. The function f is crucial for design purposes and will be defined shortly.
Write

$$P(\lambda, s) = P_m(\lambda, s)\, P_a(\lambda, s) ,$$

where $P_m(\lambda, s)$ is minimum phase and $P_a(\lambda, s)$ is all-pass. Let $P_{m0}(s)$ be the minimum phase nominal plant model and $P_{a0}(s)$ be the all-pass nominal plant model. Let

$$P_0(s) = P_{m0}(s) \cdot P_{a0}(s) .$$

Define:

$$L_0(s) = L_{m0}(s) \cdot P_{a0}(s) = P_{m0}(s)\, G(s) . P_{a0}(s)$$

$$\eta(\omega, \lambda, G(i\omega)) \le 1 \Leftrightarrow \left| \frac{P_0(i\omega)}{P(\lambda, i\omega)\, P_{a0}(i\omega)} + L_{m0}(i\omega) \right| - W_2(\omega) |L_{m0}(i\omega)| \ge W_1(\omega) \left| \frac{P_0(i\omega)}{P(\lambda, i\omega)} \right| \tag{7}$$

$$\forall\ \lambda \in \Lambda\ ,\ \forall\ \omega \in [0, \infty]$$

By defining:

$$p(\lambda, \omega)\, e^{i\theta(\lambda, \omega)} = \frac{P_0(i\omega)}{P(\lambda, i\omega) P_{a0}(i\omega)} , \quad \text{and } L_{m0}(i\omega) = q(\omega)\, e^{i\phi(\omega)} ,$$

the above inequality, (dropping the argument ω), reduces to:

$$\begin{aligned} f(\omega, \phi, W_1, W_2, q) = & \left(1 - W_2^2\right) q^2 + 2p(\lambda)\left(\cos(\theta(\lambda) - \phi) - W_1 W_2\right) q \\ & + \left(1 - W_1^2\right) p^2(\lambda) \ge 0 , \forall \lambda \in \Lambda , \forall \omega . \end{aligned} \tag{8}$$

At each ω, one solves the above parabolic inequality as a quadratic equation for a grid of various $\lambda \in \Lambda$. By examining the solutions over $\phi \in [-2\pi, 0]$, one determines a boundary

$$\partial Cp(\omega, \phi) = \{P_0 G : \bar{\eta}(\omega, G(i\omega)) = 1\} \subset \mathbf{C} ,$$

so that

$$\partial\Gamma(\omega, G(i\omega)) = \partial Cp(\omega, \phi) .$$

Let the interior of this boundary be $\overset{o}{C}p(\omega,\phi) \subset \mathbf{C}$ . Then for $W_2 \le 1$, it can be shown that (Bondarev et al., 1985; Tabarrok & Tong, 1993; Esmailzadeh et al., 1990):

$$\Gamma\left(\omega,G(i\omega)\right) = \mathbf{C} \setminus \overset{o}{C}p(\omega,\phi) = \left\{P_0 G : \bar{\eta}\left(\omega,G(i\omega)\right) \le 1\right\} , \tag{9}$$

while for $W_2 > 1$

$$\Gamma\left(\omega,G(i\omega)\right) = \partial Cp(\omega,\phi) \cup \overset{o}{C}p(\omega,\phi) = Cp(\omega,\phi).$$

In this way both the level curves $\partial\Gamma\left(\omega,G(i\omega)\right)$ as well as the sub level sets $\Gamma\left(\omega,G(i\omega)\right)$ can be computed $\forall\ \omega \in [0,\infty]$. Let **N** represent the Nichols' plane:

$$\mathbf{N} = \left\{(\phi,\mathbf{r}) : -2\pi \le \phi \le 0\ ,\ -\infty < r < \infty\right\}$$

If $s = qe^{i\phi}$, then the map $L_m : s \to \mathbf{N}$ sends s to **N** by the formula:

$$L_m s = r + i\phi = 20 \log(qe^{i\phi}) = 20 \log q + i\phi \ . \tag{10}$$

Consequently, $L_m : \partial\Gamma\left(\omega,G(i\omega)\right) \to \partial Bp(\omega,\phi,20\log q)$

converts the level curves to boundaries on the Nichols' plane called design bounds. These design bounds are identical to the traditional QFT design bounds except that unlike the QFT bounds, $\partial\Gamma\left(\omega,G(i\omega)\right)$ can be used to generate $\partial Bp\ \ \forall\ \omega \in [0,\infty]$ whereas in traditional QFT, this is possible only up to a certain $\omega = \omega_h < \infty$. This clearly shows that every admissible finite order rational approximation is necessarily sub-optimal. This is the essence of all QFT based design methods.

According to the optimization theorem, if a solution to the problem exists, then there is an optimal minimum phase loop transmission function: $L^*_{m0}(i\omega) = P_{m0}(i\omega) \cdot G^*(i\omega)$ which satisfies

$$\bar{\eta}\left(\omega,G^*(i\omega)\right) = 1\ ,\ \forall\omega \in [0,\infty] \tag{11}$$

such $|L^*_{m0}| = q^*(\omega)$, gives $20 \log\ q^*(\omega)$ which lies on $\partial Bp$ , $\forall\ \omega \in [0,\infty]$. If $q^*(\omega)$ is found, then (Robinson, 1962) if $W_1(\omega) \in L_1$ and $W_2^{-1}(\omega) \in L_2$; it follows that

$$L^*_{m0}(s) = \exp\left[\frac{1}{\pi}\int_{-\infty}^{\infty} \frac{1 - i\alpha s}{s - i\alpha} \log \frac{q^*(\alpha)}{1+\alpha^2}\ d\alpha\right] \in H_2 \ . \tag{12}$$

Clearly $L^*_{m0}(s)$ is non-rational and every admissible finite order rational approximation of it is necessarily sub-optimal; and is the essence of all QFT based design methods.

However, this sub-optimality enables the designer to address structural stability issues by proper choice of the poles and zeros of any admissible approximation G(s). Without control of the locations of the poles and zeros of G(s), singularities could result in the closed loop

characteristic polynomial. Sub-optimality also enables us to back off from the non-realizable unique optimal solution to a class of admissible solutions which because of the compactness and connectedness of $\Lambda$ (which is a differentiable manifold), induce genericity of the resultant solutions. After this, one usually optimizes the resulting controller so as to obtain quality adequacy (Thompson, 1998).

### 2.2 Design algorithm: Systematic loop-shaping

The design theory developed in section 2.1, now leads directly to the following systematic design algorithm:

1. Choose a sufficient number of discrete frequency points:

$$\omega_1, \omega_2 \ldots \omega_N < \infty.$$

2. Generate the level curves $\partial\, \Gamma(\omega_i, G(i\omega))$ and translate them to the corresponding bounds $\partial\, \beta_p(\omega_i, \phi)$.
3. With fixed controller order $n_G$, use the QFT design methodology to fit a loop transmission function $L_{m_0}(i\omega)$, to lie just on the correct side of each boundary $\partial\, \beta_p(\omega_i, \phi)$ at its frequency $\omega_i$, for $-2\pi \le \phi \le 0$ (start with $n_G = 1\ or\ 2$).
4. If step 3 is feasible, continue, otherwise go to 7.
5. Determine the information content (of G(s)) $I_c$, and apply some nonlinear local optimization algorithm to minimize $I_c$ until further reduction is not feasible without violating the bounds $\partial\, \beta_p(\omega_i, \phi)$. This is an iterative process.
6. Determine $C_r$. If $C_r \le 1$, go to 8, otherwise continue.
7. Increase $n_G$ by 1 (i.e., set $n_G = n_G + 1$) and return to 3.
8. End.

At the end of the algorithm, we obtain a feasible minimal order, minimal information content, and quality-adequate controller.

**Design Example**

Consider:

$$P(\lambda, s)\left[1 + \Delta\right] = \frac{k(1 - bs)}{s(1 + ds)}\,(1+\Delta) \quad , \quad \lambda = \left[k, b, d\right]^T \in \Lambda \ .$$

$$\mathrm{k} \in [1, 3] \ , \ \mathrm{b} \in [0.05, 0.1] \ , \ \mathrm{d} \in [0.3, 1]$$

$$P_0(s) = \frac{3(1 - 0.05s)}{s(1 + 0.35)} \quad |\Delta| < |W_2| \ .$$

$$W_1(s) = \frac{s + 1.8}{2.80s} \quad \text{and} \quad W_2(s) = \frac{2(0.0074s^3 + 0.333s^2 + 1.551s + 1)\,(.00001s + 1)}{3(0.0049s^3 + 0.246s^2 + 1.157s + 1)}$$

$W_1(s) \notin RH^\infty$ but $W_2^1(s) \in RH^2$. Since we are dealing with loop-shaping, that $W_1, \notin RH^\infty$ does not matter (Nordgren et al., 1995).

Using the scheme just described, the first feasible controller G(s) was found as:

$$G(s) = \frac{83.94\ (s + 0.66)\,(s + 1.74)\,(s + 4.20)}{(s + 0.79)\,(s + 2.3)\ (s + 8.57)\,(s + 40)}.$$

This controller produced: $I_c = 206$, and $C_r = 39.8$. Although $X(\lambda_0, s)$ is now structurally stable, $C_r$ is still large and could generate large spectral sensitivity due to its large modal matrix condition number $\kappa(V)$.

Because reduction of the information content improves quality adequacy, Thompson (Thompson, 1998) employed the nonlinear programming optimization routine to locally optimize the parameters of G(s) so as to further reduce its information content, and obtained the optimized controller:

$$\bar{G}(s) = \frac{34.31\ (s + 0.5764)\,(s + 2.088)\,(s + 5.04)}{(s + 0.632)\,(s + 1.84)\ (s + 6.856)\,(s + 40)}.$$

This optimized controller now produced: $I_c = 0$, and $C_r = 0.925$.

Note that the change in pole locations in both cases is highly insignificant. However, because of the large coefficients associated with the un-optimized polynomial it is not yet quality-adequate, and has $C_r = 39.8$. The optimized polynomial on the other hand has the pleasantly small $C_r = 0.925$, thus resulting in a quality adequate design. For solving the $\alpha(\lambda)$ singularity problem, structural stability of $X(\lambda_0, s)$ is enough. However, to solve the other spectral sensitivity problems, $C_r \leq 1$ is required. We have so far failed to obtain a quality-adequate design from any of the modern optimal methods $(\ell_1, H_2, H^\infty, \mu)$.

Quality adequacy is demanded of most engineering designs. For linear control system designs, this translates to quality- adequate closed loop characteristic polynomials under small plant and/or controller perturbations (both parametric and non parametric). Under these conditions, all optimization based designs produce quality inadequate closed loop polynomials. By backing off from these unique non-generic optimal solutions, one can produce a family of quality-adequate solutions, which are in tune with modern engineering design methodologies. These are the solutions which practical engineers desire and can confidently implement. The major attraction of the optimization-based design methods is that they are both mathematically elegant and tractable, but no engineering designer ever claims that real world design problems are mathematically beautiful. We suggest that, like in all other design areas, quality adequacy should be added as an extra condition on all feedback design problems. Note that if we follow axiomatic design theory, every MIMO problem should be broken up into a series of SISO sub-problems. This is why we have not considered the MIMO problem herein.

## 3. Sliding mode control preliminaries

In sliding mode control, a time varying surface of $S$(t) is defined with the use of a desired vector, $X_d$, and the name is given as the sliding surface. If the state vector $X$ can remain on the surface $S$(t) for all time, t>0, tracking can be achieved. In other words, problem of tracking the state vector, $X \equiv X_d$ (n- dimensional desired vector) is solved. Scalar quantity, $s$,

is the distance to the sliding surface and this becomes zero at the time of tracking. This replaces the vector $X_d$ effectively by a first order stabilization problem in $s$. The scalar $s$ represents a realistic measure of tracking performance since bounds on $s$ and the tracking error vector are directly connected. In designing the controller, a feedback control law $U$ can be chosen appropriately to satisfy sliding conditions. The control law across the sliding surface can be made discontinuous in order to facilitate for the presence of modeling imprecision and of disturbances. Then the discontinuous control law $U$ is smoothed accordingly using QFT to achieve an optimal trade-off between control bandwidth and tracking precision.

Consider the second order single-input dynamic system (Jean-Jacques & Weiping, 1991)

$$\ddot{x} = f(X) + b(X)U \ , \tag{13}$$

where

$X$ – State vector, $[\, x \ \ \dot{x} \,]^{\mathrm{T}}$

$x$ – Output of interest

$f$ - Nonlinear time varying or state dependent function

$U$ – Control input torque

$b$ – Control gain

The control gain, $b$, can be time varying or state-dependent but is not completely known. In other words, it is sufficient to know the bounding values of $b$,

$$0 < b_{\min} \le b \le b_{\max} \ . \tag{14}$$

The estimated value of the control gain, $b_{\mathrm{es}}$, can be found as (Jean-Jacques & Weiping, 1991)

$$b_{\mathrm{es}} = (b_{\min} b_{\max})^{1/2}$$

Bounds of the gain $b$ can be written in the form:

$$\beta^{-1} \le \frac{b_{es}}{b} \le \beta \tag{15}$$

Where

$$\beta = \left[ \frac{b_{\max}}{b_{\min}} \right]^{1/2}$$

The nonlinear function $f$ can be estimated ($f_{\mathrm{es}}$) and the estimation error on $f$ is to be bounded by some function of the original states of $f$.

$$\left| f_{es} - f \right| \le F \tag{16}$$

In order to have the system track on to a desired trajectory $x(t) \equiv x_d(t)$, a time-varying surface, $S$(t) in the state-space $R^2$ by the scalar equation $s$(x;t) = $s$ = 0 is defined as

$$s = \left( \frac{d}{dt} + \lambda \right) \bar{x} = \dot{\bar{x}} + \lambda \bar{x} \tag{17}$$

where $\bar{X} = X - X_d = \left[\bar{x} \;\; \dot{\bar{x}}\right]^T$

and $\lambda$ = positive constant (first order filter bandwidth)

When the state vector reaches the sliding surface, $S$(t), the distance to the sliding surface, $s$, becomes zero. This represents the dynamics while in sliding mode, such that

$$\dot{s} = 0 \tag{18}$$

When the Eq. (9) is satisfied, the equivalent control input, $U_{es}$, can be obtained as follows:

$$b \to b_{es}$$

$$b_{es}\, U \to U_{es}$$

$$f \to f_{es,}$$

This leads to

$$U_{es} = - f_{es} + \ddot{x}_d - \lambda\dot{\bar{x}}\,, \tag{19}$$

and $U$ is given by

$$U = \left(\frac{1}{b_{es}}\right)\left(U_{es} - k(x)\mathrm{sgn}(s)\right)$$

where

$k(x)$ is the control discontinuity.

The control discontinuity, $k(x)$ is needed to satisfy sliding conditions with the introduction of an estimated equivalent control. However, this control discontinuity is highly dependent on the parametric uncertainty of the system. In order to satisfy sliding conditions and for the system trajectories to remain on the sliding surface, the following must be satisfied:

$$\frac{1}{2}\frac{d}{dt}s^2 = s\dot{s} \le - \eta|s| \tag{20}$$

where $\eta$ is a strictly positive constant.

The control discontinuity can be found from the above inequality:

$$s\left[(f - bb_{es}^{-1}f_{es}) + (1 - bb_{es}^{-1})(-\ddot{x}_d + \lambda\dot{\bar{x}}) - bb_{es}^{-1}k(x)\mathrm{sgn}(s)\right] \le -\eta|s|$$

$$s\left[(f - bb_{es}^{-1}f_{es}) + (1 - bb_{es}^{-1})(-\ddot{x}_d + \lambda\dot{\bar{x}})\right] + \eta|s| \le bb_{es}^{-1}k(x)|s|$$

$$k(x) \ge \frac{s}{|s|}\left[b_{es}b^{-1}f - f_{es} + (b_{es}b^{-1} - 1)(-\ddot{x}_d + \lambda\dot{\bar{x}})\right] + b_{es}b^{-1}\eta$$

For the best tracking performance, $k(x)$ must satisfy the inequality

$$k(x) \ge \left|b_{es}b^{-1}f - f_{es} + (b_{es}b^{-1} - 1)(-\ddot{x}_d + \lambda\dot{\bar{x}})\right| + b_{es}b^{-1}\eta$$

As seen from the above inequality, the value for $k(x)$ can be simplified further by rearranging $f$ as below:

$$f = f_{es} + (f - f_{es}) \text{ and } |f_{es} - f| \le F$$

$$k(x) \ge |b_{es} b^{-1}(f - f_{es}) + (b_{es}b^{-1} - 1)(f_{es} - \ddot{x}_d + \lambda\dot{\tilde{x}})| + b_{es}b^{-1}\eta$$

$$k(x) \ge |b_{es} b^{-1}(f - f_{es})| + |b_{es}b^{-1} - 1)(f_{es} - \ddot{x}_d + \lambda\dot{\tilde{x}}| + b_{es}b^{-1}\eta$$

$$k(x) \ge \beta(F + \eta) + (\beta - 1)|(f_{es} - \ddot{x}_d + \lambda\dot{\tilde{x}}|$$

$$k(x) \ge \beta(F + \eta) + (\beta - 1)|U_{es}| \tag{21}$$

By choosing $k(x)$ to be large enough, sliding conditions can be guaranteed. This control discontinuity across the surface $s = 0$ increases with the increase in uncertainty of the system parameters. It is important to mention that the functions for $f_{es}$ and $F$ may be thought of as any measured variables external to the system and they may depend explicitly on time.

### 3.1 Rearrangement of the sliding surface

The sliding condition $\dot{s} = 0$ does not necessarily provide smooth tracking performance across the sliding surface. In order to guarantee smooth tracking performance and to design an improved controller, in spite of the control discontinuity, sliding condition can be redefined, i.e. $\dot{s} = -\alpha s$ (Taha et al., 2003), so that tracking of $x \to x_d$ would achieve an exponential convergence. Here the parameter $\alpha$ is a positive constant. The value for $\alpha$ is determined by considering the tracking smoothness of the unstable system. This condition modifies $U_{es}$ as follows:

$$U_{es} = -f_{es} + \ddot{x}_d - \lambda\dot{\tilde{x}} - \alpha s$$

and $k(x)$ must satisfy the condition

$$k(x) \ge |b_{es}b^{-1}f - f_{es} + (b_{es}b^{-1} - 1)(-\ddot{x}_d + \lambda\dot{\tilde{x}})| + b_{es}b^{-1}\eta - \alpha|s|$$

Further $k(x)$ can be simplified as

$$k(x) \ge \beta(F + \eta) + (\beta - 1)|U_{es}| + (\beta - 2)\,\alpha|s| \tag{22}$$

Even though the tracking condition is improved, chattering of the system on the sliding surface remains as an inherent problem in SMC. This can be removed by using QFT to follow.

### 3.2 QFT controller design

In the previous sections of sliding mode preliminaries, designed control laws, which satisfy sliding conditions, lead to perfect tracking even with some model uncertainties. However,

after reaching the boundary layer, chattering of the controller is observed because of the discontinuity across the sliding surface. In practice, this situation can extremely complicate designing hardware for the controller as well as affect desirable performance because of the time lag of the hardware functionality. Also, chattering excites undesirable high frequency dynamics of the system. By using a QFT controller, the switching control laws can be modified to eliminate chattering in the system since QFT controller works as a robust low pass filter. In QFT, attraction by the boundary layer can be maintained for all $t > 0$ by varying the boundary layer thickness, $\phi$ , as follows:

$$|s| \geq \phi \rightarrow \frac{1}{2}\frac{d}{dt}s^2 \leq (\dot{\phi} - \eta)|s| \tag{23}$$

It is evident from Eq. (23) that the boundary layer attraction condition is highly guaranteed in the case of boundary layer contraction ( $\dot{\phi} < 0$ ) than for boundary layer expansion ( $\dot{\phi} > 0$ ) (Jean-Jacques, 1991). Equation (23) can be used to modify the control discontinuity gain, $k(x)$, to smoothen the performance by putting $\bar{k}(x)\text{sat}(s/\phi)$ instead of $k(x)\text{sgn}(s)$. The relationship between $\bar{k}(x)$ and $k(x)$ for the boundary layer attraction condition can be presented for both the cases as follows:

$$\phi > 0 \rightarrow \bar{k}(x) = k(x) - \phi \ /\beta^2 \tag{24}$$

$$\phi < 0 \rightarrow \bar{k}(x) = k(x) - \phi \ \beta^2 \tag{25}$$

Then the control law, $U$, and $\dot{s}$ become

$$U = \left(\frac{1}{b_{es}}\right)\left(U_{es} - \bar{k}(x)\text{sat}(s/\phi)\right)$$

$$\dot{s} = -bb_{es}^{-1}(\bar{k}(x)\text{sat}(s/\phi) + \alpha s) + \Delta g(x, x_d)$$

Where $\Delta g(x, x_d) = (f - bb_{es}^{-1} f_{es}) + (1 - bb_{es}^{-1})(-\ddot{x}_d + \lambda\dot{\tilde{x}})$

Since $\bar{k}(x)$ and $\Delta g$ are continuous in $x$, the system trajectories inside the boundary layer can be expressed in terms of the variable $s$ and the desired trajectory $x_d$ by the following relation: Inside the boundary layer, i.e.,

$$|s| \leq \phi \rightarrow \text{sat}(s/\phi) = s/\phi \ \text{ and } x \rightarrow x_d \, .$$

Hence

$$\dot{s} = -\beta_d^2(\bar{k}(x_d)(s/\phi) + \ \alpha s) + \Delta g(x_d) \, . \tag{26}$$

$$\text{Where} \quad \beta_d = \left[\frac{b_{es}(x_d)_{\max}}{b_{es}(x_d)_{\min}}\right]^{1/2} .$$

The dynamics inside the boundary layer can be written by combining Eq. (24) and Eq. (25) as follows:

$$\dot{\phi} > 0 \rightarrow \bar{k}(x_d) = k(x_d) - \dot{\phi} / \beta_d^2 \tag{27}$$

$$\dot{\phi} < 0 \rightarrow \bar{k}(x_d) = k(x_d) - \dot{\phi} / \beta_d^2 \tag{28}$$

By taking the Laplace transform of Eq. (26), It can be shown that the variable $s$ is given by the output of a first-order filter, whose dynamics entirely depends on the desired state $x_d$ (Fig.1).

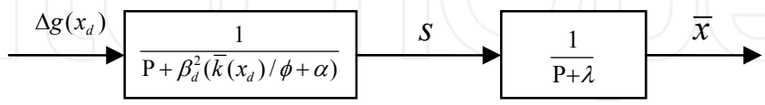


$\phi$ selection $s$ selection

Fig. 1. Structure of closed-loop error dynamics

Where P is the Laplace variable. $\Delta g(x_d)$ are the inputs to the first order filter, but they are highly uncertain.

This shows that chattering in the boundary layer due to perturbations or uncertainty of $\Delta g(x_d)$ can be removed satisfactorily by first order filtering as shown in Fig.1 as long as high-frequency unmodeled dynamics are not excited. The boundary layer thickness, $\phi$, can be selected as the bandwidth of the first order filter having input perturbations which leads to tuning $\phi$ with $\lambda$:

$$\bar{k}(x_d) = (\lambda / \beta_d^2 - \alpha)\phi \tag{29}$$

Combining Eq. (27) and Eq. (29) yields

$$k(x_d) > \phi(\lambda / \beta_d^2 - \alpha) \text{ and } \dot{\phi} + (\lambda - \alpha\beta_d^2)\phi = \beta_d^2 k(x_d) \tag{30}$$

Also, by combining Eq. (28) and Eq. (29) results in

$$k(x_d) < \phi(\lambda / \beta_d^2 - \alpha) \text{ and } \dot{\phi} + (\phi / \beta_d^2)\left[(\lambda / \beta_d^2) - \alpha\right] = k(x_d) / \beta_d^2 \tag{31}$$

Equations (24) and (30) yield

$$\dot{\phi} > 0 \rightarrow \bar{k}(x) = k(x) - (\beta_d / \beta)^2 [k(x_d) - \phi(\lambda / \beta_d^2 - \alpha)] \tag{32}$$

and combining Eq. (22) with Eq. (28) gives

$$\dot{\phi} < 0 \rightarrow \bar{k}(x) = k(x) - (\beta / \beta_d)^2 [k(x_d) - \phi(\lambda / \beta_d^2 - \alpha)] \tag{33}$$

In addition, initial value of the boundary layer thickness, $\phi(0)$, is given by substituting $x_d$ at t=0 in Eq. (29).

$$\phi(0) = \frac{\bar{k}(x_d(0))}{(\lambda / \beta_d^2) - \alpha}$$

The results discussed above can be used for applications to track and stabilize highly nonlinear systems. Sliding mode control along with QFT provides better system controllers and leads to selection of hardware easier than using SMC alone. The application of this theory to a driver seat of a heavy vehicle and its simulation are given in the following sections.

## 4. Numerical example

In this section, the sliding mode control theory is applied to track the motion behavior of a driver's seat of a heavy vehicle along a trajectory that can reduce driver fatigue and drowsiness. The trajectory can be varied accordingly with respect to the driver requirements. This control methodology can overcome most of the road disturbances and provide predetermined seat motion pattern to avoid driver fatigue. However, due to parametric uncertainties and modeling inaccuracies chattering can be observed which causes a major problem in applying SMC alone. In general, the chattering enhances the driver fatigue and also leads to premature failure of controllers. SMC with QFT developed in this chapter not only eliminates the chattering satisfactorily but also reduces the control effort necessary to maintain the desired motion of the seat.

Relationship between driver fatigue and seat vibration has been discussed in many publications based on anecdotal evidence (Wilson & Horner, 1979; Randall, 1992). It is widely believed and proved in field tests that lower vertical acceleration levels will increase comfort level of the driver (U. & R. Landstorm, 1985; Altunel, 1996; Altunel & deHoop, 1998). Heavy vehicle truck drivers who usually experience vibration levels around 3 Hz, while driving, may undergo fatigue and drowsiness (Mabbott et al., 2001). Fatigue and drowsiness, while driving, may result in loss of concentration leading to road accidents. Human body metabolism and chemistry can be affected by intermittent and random vibration exposure resulting in fatigue (Kamenskii, 2001). Typically, vibration exposure levels of heavy vehicle drivers are in the range 0.4 $m/s^2$ - 2.0 $m/s^2$ with a mean value of 0.7 $m/s^2$ in the vertical axis (U. & R. Landstorm, 1985; Altunel, 1996; Altunel & deHoop, 1998; Mabbott et al., 2001).

A suspension system determines the ride comfort of the vehicle and therefore its characteristics may be properly evaluated to design a proper driver seat under various operating conditions. It also improves vehicle control, safety and stability without changing the ride quality, road holding, load carrying, and passenger comfort while providing directional control during handling maneuvers. A properly designed driver seat can reduce driver fatigue, while maintaining same vibration levels, against different external disturbances to provide improved performance in riding.

Over the past decades, the application of sliding mode control has been focused in many disciplines such as underwater vehicles, automotive applications and robot manipulators (Taha et al., 2003; Roberge, 1960; Dorf, 1967; Ogata, 1970; Higdon, 1963; Truxal, 1965; Lundberg, 2003; Phillips, 1994; Siebert, 1986). The combination of sliding controllers with state observers was also developed and discussed for both the linear and nonlinear cases (Hedrick & Gopalswamy, 1989; Bondarev et al., 1985). Nonlinear systems are difficult to model as linear systems since there are certain parametric uncertainties and modeling inaccuracies that can eventually resonate the system (Jean-Jacques, 1991). The sliding mode control can be used for nonlinear stabilization problems in designing controllers. Sliding mode control can provide high performance systems that are robust to parameter

uncertainties and disturbances. Design of such systems includes two steps: (i) choosing a set of switching surfaces that represent some sort of a desired motion, and (ii) designing a discontinuous control law that ensures convergence to the switching surfaces (Dorf, 1967; Ogata, 1970). The discontinuous control law guarantees the attraction features of the switching surfaces in the phase space. Sliding mode occurs when the system trajectories are confined to the switching surfaces and cannot leave them for the remainder of the motion. Although this control approach is relatively well understood and extensively studied, important issues related to implementation and chattering behavior remain unresolved. Implementing QFT during the sliding phase of a SMC controller not only eliminates chatter but also achieves vibration isolation. In addition, QFT does not diminish the robustness characteristics of the SMC because it is known to tolerate large parametric and phase information uncertainties.

Figure 2 shows a schematic of a driver seat of a heavy truck. The model consists of an actuator, spring, damper and a motor sitting on the sprung mass. The actuator provides actuation force by means of a hydraulic actuator to keep the seat motion within a comfort level for any road disturbance, while the motor maintains desired inclination angle of the driver seat with respect to the roll angle of the sprung mass. The driver seat mechanism is connected to the sprung mass by using a pivoted joint; it provides the flexibility to change the roll angle. The system is equipped with sensors to measure the sprung mass vertical acceleration and roll angle. Hydraulic pressure drop and spool valve displacement are also used as feedback signals.

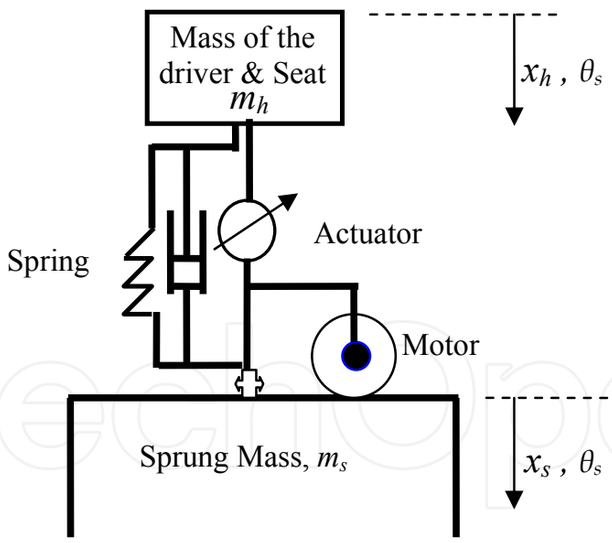


Fig. 2. The hydraulic power feed of the driver seat on the sprung mass

**Nomenclature**

$A$ - Cross sectional area of the hydraulic actuator piston
$F_{af}$ - Actuator force
$F_h$ - Combined nonlinear spring and damper force of the driver seat
$k_h$ - Stiffness of the spring between the seat and the sprung mass

$m_h$ - Mass of the driver and the seat
$m_s$ - Sprung mass
$x_h$ - Vertical position coordinate of the driver seat
$x_s$ - Vertical position coordinate of the sprung mass
$\theta_s$ - Angular displacement of the driver seat (same as sprung mass)

### 4.1 Equations of motion

Based on the mathematical model developed above, the equation of motion in the vertical direction for the driver and the seat can be written as follows:

$$\ddot{x}_h = -(1/m_h)F_h + (1/m_h)F_{af}\,, \tag{34}$$

where

$$F_h = k_{h1}d_h + k_{h2}d_h^3 + C_{h1}\dot{d}_h + C_{h2}\dot{d}_h^2\,\mathrm{sgn}(\dot{d}_h)$$

$k_{h1}$ - linear stiffness
$k_{h2}$ - cubic stiffness
$C_{h1}$ - linear viscous damping
$C_{h2}$ - fluidic (amplitude dependent) damping
sgn - signum function

$$F_{af} = AP_L$$

$$d_h = (x_h - x_s) - a_{1i}\sin\theta_s$$

Complete derivation of Eq. (34) is shown below for a five-degree-of-freedom roll and bounce motion configuration of the heavy truck driver-seat system subject to a sudden impact. In four-way valve-piston hydraulic actuator system, the rate of change of pressure drop across the hydraulic actuator piston, $P_L$, is given by (Fialho, 2002)

$$\frac{V_1\dot{P}_L}{4\beta_e} = Q - C_{lp}P_L - A(\dot{x}_h - \dot{x}_s) \tag{35}$$

$V_t$ - Total actuator volume
$b_e$ - Effective bulk modulus of the fluid
$Q$ - Load flow
$C_{tp}$ - Total piston leakage coefficient
$A$ - Piston area
The load flow of the actuator is given by (Fialho, 2002):

$$Q = \mathrm{sgn}\left[P_s - \mathrm{sgn}(x_v)P_1\right]C_d\omega x_v\sqrt{(1/\rho)\left|P_s - \mathrm{sgn}(x_v)P_L\right|} \tag{36}$$

$P_s$ – Hydraulic supply pressure
ω - Spool valve area gradient
$X_v$ – Displacement of the spool valve

ρ - Hydraulic fluid density
$C_d$ – Discharge coefficient
Voltage or current can be fed to the servo-valve to control the spool valve displacement of the actuator for generating the force. Moreover, a stiction model for hydraulic spool can be included to reduce the chattering further, but it is not discussed here.

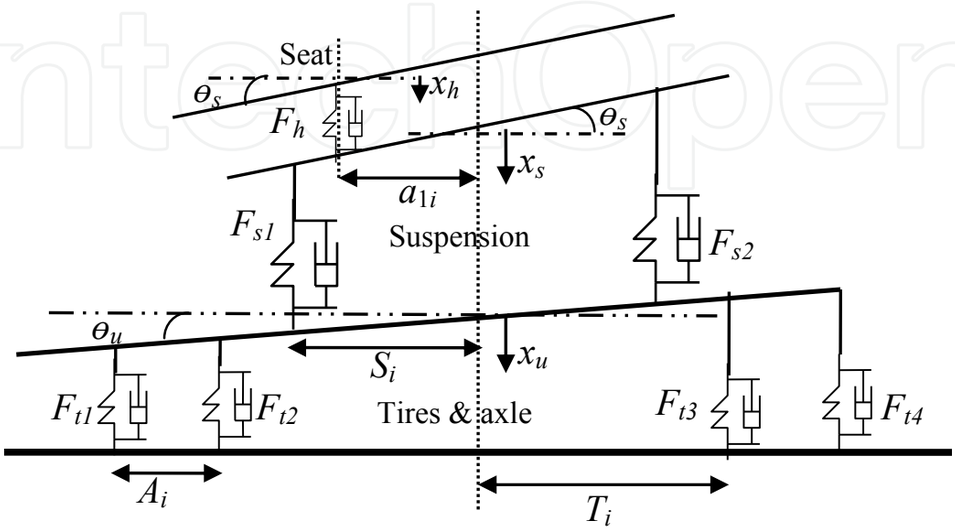


Fig. 3. Five-degree-of-freedom roll and bounce motion configuration of the heavy duty truck driver-seat system.

**Nonlinear force equations**

Nonlinear tire forces, suspension forces, and driver seat forces can be obtained by substituting appropriate coefficients to the following nonlinear equation that covers wide range of operating conditions for representing dynamical behavior of the system.

$$F = k_1 d + k_2 d^3 + C_1 \dot{d} + C_2 \dot{d}^2 \operatorname{sgn}(\dot{d})$$

where
$F$ - Force
$k_1$ - linear stiffness coefficient
$k_2$ - cubic stiffness coefficient
$C_1$ - linear viscous damping coefficient
$C_2$ - amplitude dependent damping coefficient
$d$ - deflection
For the suspension:

$$F_{si} = k_{si1} d_{si} + k_{si2} d_{si}^3 + C_{si1} \dot{d}_{si} + C_{si2} \dot{d}_{si}^2 \operatorname{sgn}(\dot{d}_{si})$$

For the tires:

$$F_{ti} = k_{ti1} d_{ti} + k_{ti2} d_{ti}^3 + C_{ti1} \dot{d}_{ti} + C_{ti2} \dot{d}_{ti}^2 \operatorname{sgn}(\dot{d}_{ti})$$

For the seat:

$$F_h = k_{h1}d_h + k_{h2}d_h^3 + C_{h1}\dot{d}_h + C_{h2}\dot{d}_h^2\,\mathrm{sgn}(\dot{d}_h)$$

**Deflection of the suspension springs and dampers**

Based on the mathematical model developed, deflection of the suspension system on the axle is found for both sides as follows:

$$\text{Deflection of side 1, } d_{s1} = (x_s - x_u) + S_i(\sin\theta_s - \sin\theta_u)$$
$$\text{Deflection of side 2, } d_{s2} = (x_s - x_u) - S_i(\sin\theta_s - \sin\theta_u)$$

**Deflection of the seat springs and dampers**

By considering the free body diagram in Fig. 3, deflection of the seat is obtained as follows (Rajapakse & Happawana, 2004):

$$d_h = (x_h - x_s) - a_{1i}\sin\theta_s$$

**Tire deflections**

The tires are modeled by using springs and dampers. Deflections of the tires to a road disturbance are given by the following equations.

$$\text{Deflection of tire 1, } d_{t1} = x_u + (T_i + A_i)\sin\theta_u$$
$$\text{Deflection of tire 2, } d_{t2} = x_u + T_i\sin\theta_u$$
$$\text{Deflection of tire 3, } d_{t3} = x_u - T_i\sin\theta_u$$
$$\text{Deflection of tire 4, } d_{t4} = x_u - (T_i + A_i)\sin\theta_u$$

**Equations of motion for the combined sprung mass, unsprung mass and driver seat**

Based on the mathematical model developed above, the equations of motion for each of the sprung mass, unsprung mass, and the seat are written by utilizing the free-body diagram of the system in Fig. 3 as follows:
Vertical and roll motion for the $i^{th}$ axle (unsprung mass)

$$m_u\ddot{x}_u = (F_{s1} + F_{s2}) - (F_{t1} + F_{t2} + F_{t3} + F_{t4}) \tag{37}$$

$$J_u\ddot{\theta}_u = S_i(F_{s1} - F_{s2})\cos\theta_u + T_i(F_{t3} - F_{t2})\cos\theta_u + (T_i + A_i)(F_{t4} - F_{t1})\cos\theta_u \tag{38}$$

Vertical and roll motion for the sprung mass

$$m_s\ddot{x}_s = -(F_{s1} + F_{s2}) + F_h \tag{39}$$

$$J_s\ddot{\theta}_s = S_i(F_{s2} - F_{s1})\cos\theta_s + a_{1i}F_h\cos\theta_s \tag{40}$$

Vertical motion for the seat

$$m_h\ddot{x}_h = -F_h \tag{41}$$

Equations (37)-(41) have to be solved simultaneously, since there are many parameters and nonlinearities. Nonlinear effects can better be understood by varying the parameters and

examining relevant dynamical behavior, since changes in parameters change the dynamics of the system. Furthermore, Eqs. (37)-(41) can be represented in the phase plane while varying the parameters of the truck, since each and every trajectory in the phase portrait characterizes the state of the truck. Equations above can be converted to the state space form and the solutions can be obtained using MATLAB. Phase portraits are used to observe the nonlinear effects with the change of the parameters. Change of initial conditions clearly changes the phase portraits and the important effects on the dynamical behavior of the truck can be understood.

### 4.2 Applications and simulations (MATLAB)

Equation (34) can be represented as,

$$\ddot{x}_h = f + bU \tag{42}$$

where

$$f = -(1/m_h)F_h$$

$$b = 1/m_h$$

$$U = F_{af}$$

The expression $f$ is a time varying function of $x_s$ and the state vector $x_h$. The time varying function, $x_s$, can be estimated from the information of the sensor attached to the sprung mass and its limits of variation must be known. The expression, $f$, and the control gain, $b$ are not required to be known exactly, but their bounds should be known in applying SMC and QFT. In order to perform the simulation, $x_s$ is assumed to vary between -0.3m to 0.3m and it can be approximated by the time varying function, $A\sin(\omega t)$, where $\omega$ is the disturbance angular frequency of the road by which the unsprung mass is oscillated. The bounds of the parameters are given as follows:

$$m_{h\min} \le m_h \le m_{h\max}$$

$$x_{s\min} \le x_s \le x_{s\max}$$

$$b_{\min} \le b \le b_{\max}$$

Estimated values of $m_h$ and $x_s$:

$$m_{hes} = \left|(m_{h\min} m_{h\max})^{1/2}\right|$$

$$x_{ses} = \left|(x_{s\min} x_{s\max})\right|^{1/2}$$

Above bounds and the estimated values were obtained for some heavy trucks by utilizing field test information (Tabarrok & Tong, 1993, 1992; Esmailzadeh et al., 1990; Aksionov, 2001; Gillespie, 1992; Wong, 1978; Rajapakse & Happawana, 2004; Fialho, 2002). They are as follows:

$m_{h\min} = 50kg$ , $m_{h\max} = 100kg$ , $x_{s\min} = -0.3m$ , $x_{s\max} = 0.3m$ , $\omega = 2\pi(0.1-10)rad/s$ , $A=0.3$

The estimated nonlinear function, *f*, and bounded estimation error, *F*, are given by:

$$f_{es} = -(k_h / m_{hes})(x_h - x_{ses})$$

$$F = \max\left| f_{es} - f \right|$$

$$b_{es} = 0.014$$

$$\beta = 1.414$$

$$x_{ses} = \left|(x_{s\min} x_{s\max})\right|^{1/2}$$

The sprung mass is oscillated by road disturbances and its changing pattern is given by the vertical angular frequency, $\omega = 2\pi(0.1 + \left|9.9\sin(2\pi t)\right|)$ . This function for $\omega$ is used in the simulation in order to vary the sprung mass frequency from 0.1 to 10 Hz. Thus $\omega$ can be measured by using the sensors in real time and be fed to the controller to estimate the control force necessary to maintain the desired frequency limits of the driver seat. Expected trajectory for $x_h$ is given by the function, $x_{hd} = B\sin\omega_d t$ , where $\omega_d$ is the desired angular frequency of the driver to have comfortable driving conditions to avoid driver fatigue in the long run. *B* and $\omega_d$ are assumed to be .05 m and $2\pi * 0.5$ rad/s during the simulation which yields 0.5 Hz continuous vibration for the driver seat over the time. The mass of the driver and seat is considered as 70 kg throughout the simulation. This value changes from driver to driver and can be obtained by an attached load cell attached to the driver seat to calculate the control force. It is important to mention that this control scheme provides sufficient room to change the vehicle parameters of the system according to the driver requirements to achieve ride comfort.

### 4.3 Using sliding mode only

In this section tracking is achieved by using SMC alone and the simulation results are obtained as follows.

Consider $x_h = x(1)$ and $\dot{x}_h = x(2)$ . Eq. (25) is represented in the state space form as follows:

$$\dot{x}(1) = x(2)$$

$$\dot{x}(2) = -(k_h / m_h)(x(1) - x_{es}) + bU$$

Combining Eq. (17), Eq. (19) and Eq. (42), the estimated control law becomes,

$$U_{es} = -f_{es} + \dot{x}_{hd} - \lambda(x(2) - \dot{x}_{hd})$$

Figures 4 to 7 show system trajectories, tracking error and control torque for the initial condition: $[x_h, \dot{x}_h]$=[0.1m , 1m/s.] using the control law. Figure 4 provides the tracked vertical displacement of the driver seat vs. time and perfect tracking behavior can be observed. Figure 5 exhibits the tracking error and it is enlarged in Fig. 6 to show it's chattering behavior after the tracking is achieved. Chattering is undesirable for the

controller that makes impossible in selecting hardware and leads to premature failure of hardware.

The values for $\lambda$ and $\eta$ in Eq. (17) and Eq. (20) are chosen as 20 and 0.1 (Jean-Jacques, 1991) to obtain the plots and to achieve satisfactory tracking performance. The sampling rate of 1 kHz is selected in the simulation. $\dot{s} = 0$ condition and the signum function are used. The plot of control force vs. time is given in Fig. 7. It is very important to mention that, the tracking is guaranteed only with excessive control forces. Mass of the driver and driver seat, limits of its operation, control bandwidth, initial conditions, sprung mass vibrations, chattering and system uncertainties are various factors that cause to generate huge control forces. It should be mentioned that this selected example is governed only by the linear equations with sine disturbance function, which cause for the controller to generate periodic sinusoidal signals. In general, the road disturbance is sporadic and the smooth control action can never be expected. This will lead to chattering and QFT is needed to filter them out. Moreover, applying SMC with QFT can reduce excessive control forces and will ease the selection of hardware.

In subsequent results, the spring constant of the tires were 1200kN/m & 98kN/m$^3$ and the damping coefficients were 300kNs/m & 75kNs/m$^2$. Some of the trucks' numerical parameters (Taha et al., 2003; Ogata, 1970; Tabarrok & Tong, 1992, 1993; Esmailzadeh et al., 1990; Aksionov, 2001; Gillespie, 1992; Wong, 1978) are used in obtaining plots and they are as follows: $m_h$ = 100kg, $m_s$ = 3300kg, $m_u$ = 1000kg, $k_{s11}$ = $k_{s21}$ = 200 kN/m & $k_{s12}$ =$k_{s22}$ = 18 kN/m$^3$, $k_{h1}$ = 1 kN/m & $k_{h2}$ = 0.03 kN/m$^3$ ,$C_{s11}$ = $C_{s21}$ = 50 kNs/m & $C_{s12}$ = $C_{s22}$ = 5 kNs/m$^2$ , $C_{h1}$ = 0.4 kNs/m & $C_{h2}$ = 0.04 kNs/m , $J_s$ = 3000 kgm$^2$ , $J_u$ = 900 kgm$^2$, $A_i$ = 0.3 m, $S_i$ = 0.9 m, and $a_{1i}$ = 0.8 m.

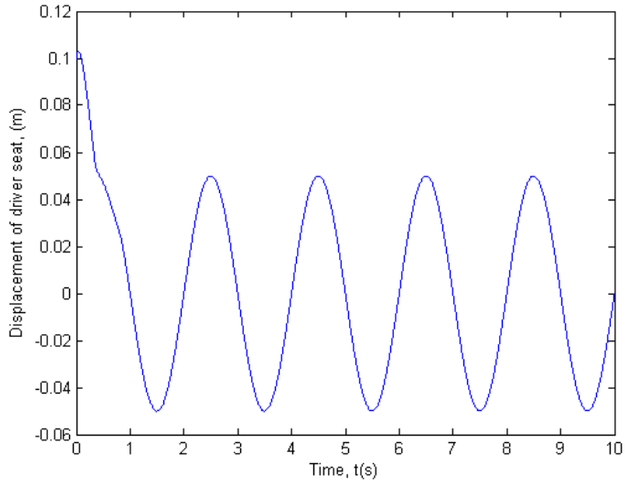


Fig. 4. Vertical displacement of driver seat vs. time using SMC only

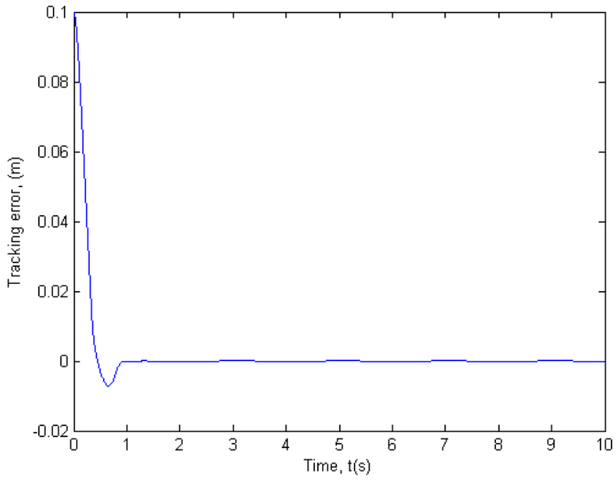


Fig. 5. Tracking error vs. time using SMC only

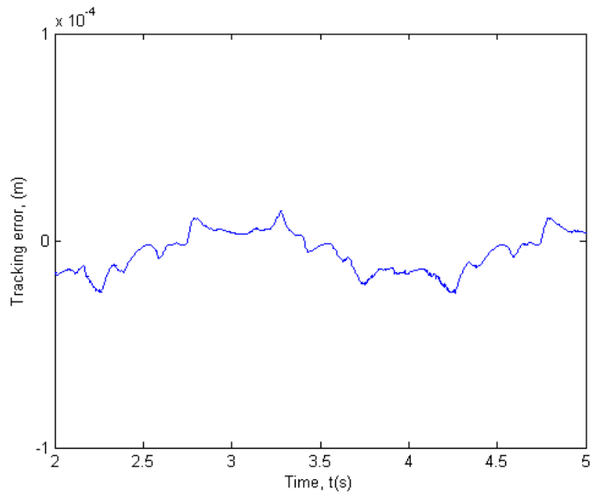


Fig. 6. Zoomed in tracking error vs. time using SMC only

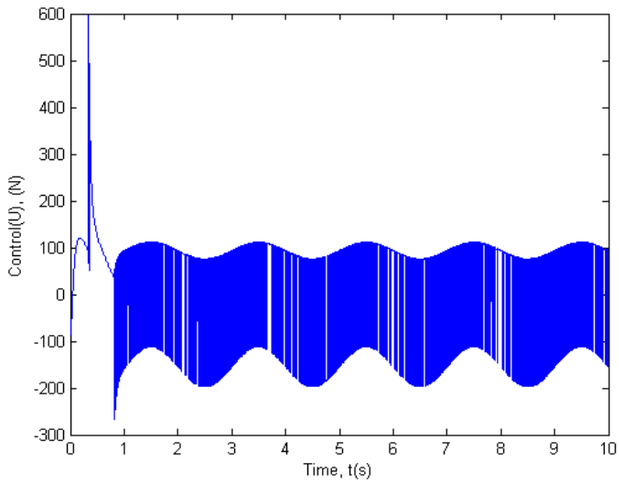


Fig. 7. Control force vs. time using SMC only

### 4.4 Use of QFT on the sliding surface

Figure 8 shows the required control force using SMC only. In order to lower the excessive control force and to further smoothen the control behavior with a view of reducing chattering, QFT is introduced inside the boundary layer. The following graphs are plotted for the initial boundary layer thickness of 0.1 meters.

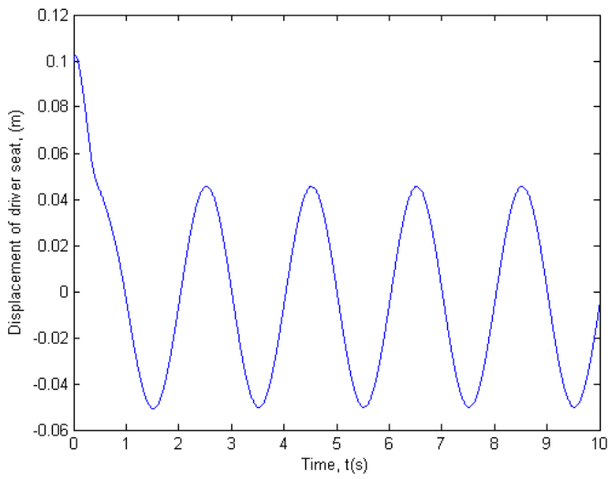


Fig. 8. Vertical displacement of driver seat vs. time using SMC & QFT

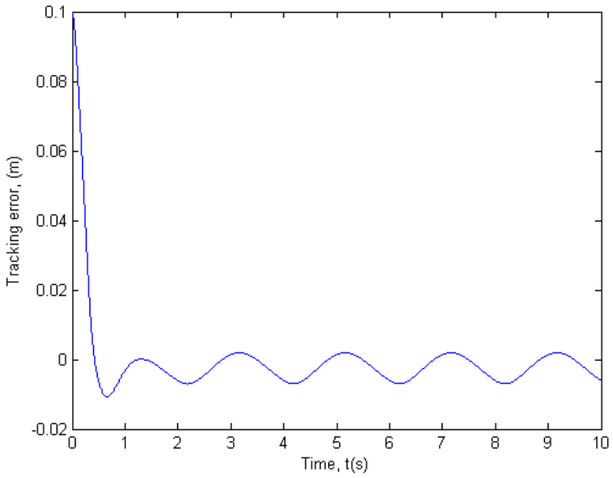


Fig. 9. Tracking error vs. time using SMC & QFT

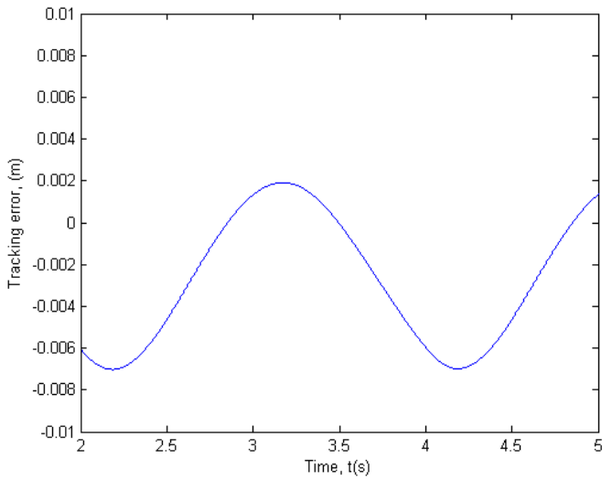


Fig. 10. Zoomed in tracking error vs. time using SMC & QFT

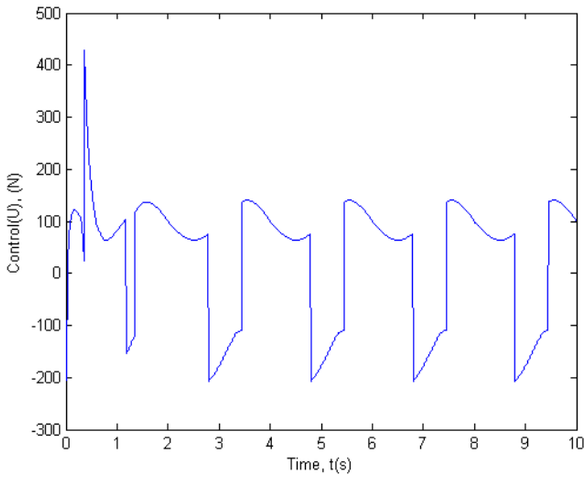


Fig. 11. Control force vs. time using SMC & QFT

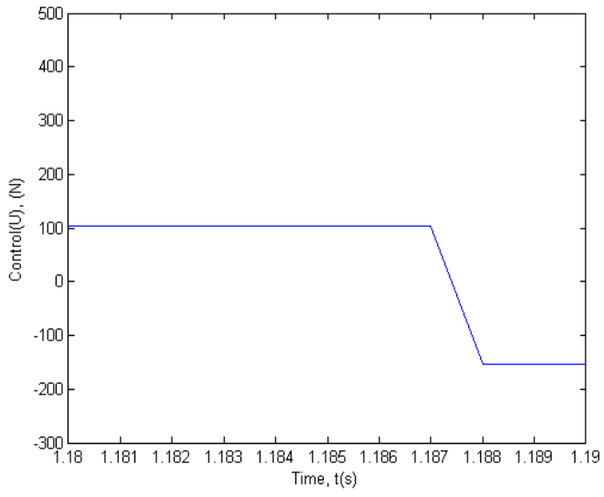


Fig. 12. Zoomed in control force vs. time using SMC & QFT

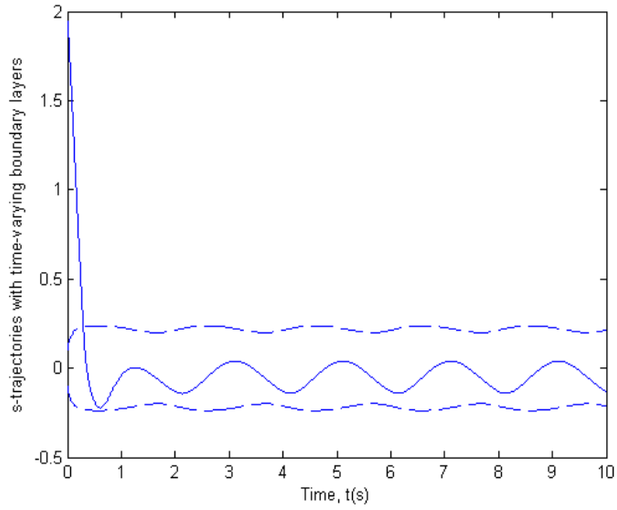


Fig. 13. s-trajectory with time-varying boundary layer vs. time using SMC & QFT

Figure 8 again shows that the system is tracked to the trajectory of interest and it follows the desired trajectory of the seat motion over the time. Figure 9 provides zoomed in tracking error of Fig. 8 which is very small and perfect tracking condition is achieved. The control force needed to track the system is given in Fig. 11. Figure 12 provides control forces for both cases, i.e., SMC with QFT and SMC alone. SMC with QFT yields lower control force and this can be precisely generated by using a hydraulic actuator. Increase of the parameter $\lambda$ will decrease the tracking error with an increase of initial control effort.

Varying thickness of the boundary layer allows the better use of the available bandwidth, which causes to reduce the control effort for tracking the system. Parameter uncertainties can effectively be addressed and the control force can be smoothened with the use of the SMC and QFT. A successful application of QFT methodology requires selecting suitable function for $F$, since the change in boundary layer thickness is dependent on the bounds of $F$. Increase of the bounds of $F$ will increase the boundary layer thickness that leads to overestimate the change in boundary layer thickness and the control effort. Evolution of dynamic model uncertainty with time is given by the change of boundary layer thickness. Right selection of the parameters and their bounds always result in lower tracking errors and control forces, which will ease choosing hardware for most applications.

## 5. Conclusion

This chapter provided information in designing a road adaptive driver's seat of a heavy truck via a combination of SMC and QFT. Based on the assumptions, the simulation results show that the adaptive driver seat controller has high potential to provide superior driver comfort over a wide range of road disturbances. However, parameter uncertainties, the presence of unmodeled dynamics such as structural resonant modes, neglected time-delays, and finite sampling rate can largely change the dynamics of such systems. SMC provides effective methodology to design and test the controllers in the performance trade-offs. Thus tracking is guaranteed within the operating limits of the system. Combined use of SMC and QFT facilitates the controller to behave smoothly and with minimum chattering that is an inherent obstacle of using SMC alone. Chattering reduction by the use of QFT supports

selection of hardware and also reduces excessive control action. In this chapter simulation study is done for a linear system with sinusoidal disturbance inputs. It is seen that very high control effort is needed due to fast switching behavior in the case of using SMC alone. Because QFT smoothens the switching nature, the control effort can be reduced. Most of the controllers fail when excessive chattering is present and SMC with QFT can be used effectively to smoothen the control action. In this example, since the control gain is fixed, it is independent of the states. This eases control manipulation. The developed theory can be used effectively in most control problems to reduce chattering and to lower the control effort. It should be mentioned here that the acceleration feedback is not always needed for position control since it depends mainly on the control methodology and the system employed. In order to implement the control law, the road disturbance frequency, $\omega$ , should be measured at a rate higher or equal to 1000Hz (comply with the simulation requirements) to update the system; higher frequencies are better. The bandwidth of the actuator depends upon several factors; i.e. how quickly the actuator can generate the force needed, road profile, response time, and signal delay, etc.

## 6. References


Aksionov, P.V. (2001). Law and criterion for evaluation of optimum power distribution to vehicle wheels, *Int. J. Vehicle Design*, Vol. 25, No. 3, pp. 198-202.

Altunel, A. O. (1996). The effect of low-tire pressure on the performance of forest products transportation vehicles, *Master's thesis*, Louisiana State University, School of Forestry, Wildlife and Fisheries.

Altunel, A. O. and De Hoop C. F. (1998). The Effect of Lowered Tire Pressure on a Log Truck Driver Seat, *Louisiana State University Agriculture Center*, Vol. 9, No. 2, Baton Rouge, USA.

Bondarev, A. G. Bondarev, S. A., Kostylyova, N. Y. and Utkin, V. I. (1985). Sliding Modes in Systems with Asymptotic State Observers, *Automatic. Remote Control*, Vol. 6.

Dorf, R. C. (1967). Modern Control Systems, *Addison-Wesley*, Reading, Massachusetts, pp. 276 – 279.

Esmailzadeh, E., Tong, L. and Tabarrok, B. (1990). Road Vehicle Dynamics of Log Hauling Combination Trucks, *SAE Technical Paper Series 912670*, pp. 453-466.

Fialho, I. and Balas, G. J. (2002). Road Adaptive Active Suspension Design Using Linear Parameter-Varying Gain-Scheduling, *IEEE transaction on Control Systems Technology*, Vol. 10, No.1, pp. 43-54.

Gillespie, T. D. (1992). *Fundamentals of Vehicle Dynamics*, SAE, Inc. Warrendale, PA.

Hedrick, J. K. and Gopalswamy, S. (1989). Nonlinear Flight Control Design via Sliding Method, Dept. of Mechanical Engineering, *Univ. of California*, Berkeley.

Higdon, D. T. and Cannon, R. H. (1963). ASME J. of the Control of Unstable Multiple-Output Mechanical Systems, *ASME Publication,* 63-WA-148, New York.

Jean-Jacques, E. S. and Weiping, L. (1991). Applied Nonlinear Control, *Prentice-Hall, Inc., Englewood Cliffs*, New Jersey 07632.

Kamenskii, Y. and Nosova, I. M. (1989). Effect of whole body vibration on certain indicators of neuro-endocrine processes, *Noise and Vibration Bulletin,* pp. 205-206.

Landstrom, U. and Landstrom, R. (1985). Changes in wakefulness during exposure to whole body vibration, *Electroencephal, Clinical, Neurophysiology*, Vol. 61, pp. 411-115.

Lundberg, K. H. and Roberge, J. K. (2003). Classical dual-inverted-pendulum control, *Proceedings of the IEEE CDC*-2003, Maui, Hawaii, pp. 4399-4404.

Mabbott, N., Foster, G. and Mcphee, B. (2001). Heavy Vehicle Seat Vibration and Driver Fatigue, Australian *Transport Safety Bureau*, Report No. CR 203, pp. 35.

Nordgren, R. E., Franchek, M. A. and Nwokah, O. D. I. (1995). A Design Procedure for the Exact $H_\infty$ SISO – Robust Performance Problem, *Int. J. Robust and Nonlinear Control*, Vol.5, 107-118.

Nwokah, O. D. I., Ukpai, U. I., Gasteneau, Z., and Happawana, G. S.(1997). Catastrophes in Modern Optimal Controllers, *Proceedings, American Control Conference*, Albuquerque, NM, June.

Ogata, K. (1970). Modern Control Engineering, *Prentice-Hall*, Englewood Cliffs, New Jersey, pp. 277 – 279.

Phillips, L. C. (1994). Control of a dual inverted pendulum system using linear-quadratic and H-infinity methods, Master's thesis, *Massachusetts Institute of Technology*.

Randall, J. M. (1992). Human subjective response to lorry vibration: implications for farm animal transport, J. *Agriculture. Engineering, Res,* Vol. 52, pp. 295-307.

Rajapakse, N. and Happawana, G. S. (2004). A nonlinear six degree-of-freedom axle and body combination roll model for heavy trucks' directional stability, *In Proceedings of IMECE2004-61851, ASME International Mechanical Engineering Congress and RD&D Expo.,* November 13-19, Anaheim, California, USA.

Roberge, J. K. (1960). The mechanical seal, *Bachelor's thesis*, Massachusetts Institute of Technology.

Siebert, W. McC. (1986) Circuits, Signals, and Systems, *MIT Press*, Cambridge, Massachusetts.

Tabarrok, B. and Tong, X. (1993). Directional Stability Analysis of Logging Trucks by a Yaw Roll Model, *Technical Reports*, University of Victoria, Mechanical Engineering Department, pp. 57- 62.

Tabarrok, B. and Tong, L. (1992). The Directional Stability Analysis of Log Hauling Truck – Double Doglogger, *Technical Reports, University of Victoria, Mechanical Engineering Department, DSC*, Vol. 44, pp. 383-396.

Taha, E. Z., Happawana, G. S., and Hurmuzlu, Y. (2003). Quantitative feedback theory (QFT) for chattering reduction and improved tracking in sliding mode control (SMC), *ASME J. of Dynamic Systems, Measurement, and Control*, Vol. 125, pp 665-669.

Thompson, D. F. (1998). Gain-Bandwidth Optimal Design for the New Formulation Quantitative Feedback Theory, *ASME J. Dyn. Syst., Meas., Control* Vol.120, pp. 401–404.

Truxal, J. G. (1965). State Models, Transfer Functions, and Simulation, Monograph 8, *Discrete Systems Concept Project*.

Wilson, L. J. and Horner, T. W. (1979). Data Analysis of Tractor-Trailer Drivers to Assess Drivers' Perception of Heavy Duty Truck Ride Quality, *Report DOT-HS-805-139, National Technical Information Service*, Springfield, VA, USA.

Wong, J.Y. (1978). Theory of Ground Vehicles*, John Wiley and Sons*.


**Recent Advances in Robust Control - Novel Approaches and Design Methods**

Edited by Dr. Andreas Mueller

ISBN 978-953-307-339-2
Hard cover, 462 pages
**Publisher** InTech
**Published online** 07, November, 2011
**Published in print edition** November, 2011

Robust control has been a topic of active research in the last three decades culminating in H_2/H_\infty and \mu design methods followed by research on parametric robustness, initially motivated by Kharitonov's theorem, the extension to non-linear time delay systems, and other more recent methods. The two volumes of Recent Advances in Robust Control give a selective overview of recent theoretical developments and present selected application examples. The volumes comprise 39 contributions covering various theoretical aspects as well as different application areas. The first volume covers selected problems in the theory of robust control and its application to robotic and electromechanical systems. The second volume is dedicated to special topics in robust control and problem specific solutions. Recent Advances in Robust Control will be a valuable reference for those interested in the recent theoretical advances and for researchers working in the broad field of robotics and mechatronics.

**How to reference**

In order to correctly reference this scholarly work, feel free to copy and paste the following:

Gemunu Happawana (2011). Quantitative Feedback Theory and Sliding Mode Control, Recent Advances in Robust Control - Novel Approaches and Design Methods, Dr. Andreas Mueller (Ed.), ISBN: 978-953-307-339-2, InTech, Available from: http://www.intechopen.com/books/recent-advances-in-robust-control-novel-approaches-and-design-methods/quantitative-feedback-theory-and-sliding-mode-control

INTECH
open science | open minds

**InTech Europe**
University Campus STeP Ri
Slavka Krautzeka 83/A
51000 Rijeka, Croatia
Phone: +385 (51) 770 447
Fax: +385 (51) 686 166
www.intechopen.com

**InTech China**
Unit 405, Office Block, Hotel Equatorial Shanghai
No.65, Yan An Road (West), Shanghai, 200040, China
中国上海市延安西路65号上海国际贵都大饭店办公楼405单元
Phone: +86-21-62489820
Fax: +86-21-62489821

IntechOpen